

# COHESIVE ZONE MODELLING OF CRACK GROWTH IN PARTICLE REINFORCED METAL MATRIX COMPOSITES

A. ROSSOLL, A. MISEREZ\* & A. MORTENSEN

Laboratory for Mechanical Metallurgy, EPFL, 1015 Lausanne, Switzerland.

\* Current affiliation: Materials Department, UCSB, Santa Barbara, CA, USA.

## ABSTRACT

Metal matrix composites have been produced by gas pressure infiltration of ceramic particle beds with pure aluminium. Two different types of alumina particles have been employed: 35  $\mu\text{m}$  angular and 15  $\mu\text{m}$  polygonal particles. The resulting composites feature a homogeneous microstructure that is free of processing defects. Crack growth in these materials was characterized via single specimen  $J$ -integral testing according to ASTM E-1737. Both types of material exhibit stable crack growth and marked  $R$ -curve behaviour. Stereophotogrammetric measurements were used in order to infer the amount of energy dissipated in the process zone, by particle cracking or and matrix voiding. In the process zone and for both types of damage, the main dissipative mechanism is via the stretching of metal ligaments.

Crack growth is modelled in CT specimens with a cohesive model, with parameters fitted from experimental load vs. CMOD records. Computed  $J$ - $\Delta a$  curves exhibit somewhat stronger crack growth as compared to experimental ones. We attribute this offset mainly to the limited sample dimensions, and to the difficulty of representing a 3-D sample with a 2-D plane strain analysis. On the other hand, the agreement is sufficiently good to confirm the metallic character of the examined half-ceramic metal matrix composites, in so far as their toughness is dominated by remote plasticity. The amplification factor in our analysis is about half as large as computed from the stereophotogrammetric measurements, but probably more reliable than the latter, which was obtained in a very simplistic analysis. Both analyses confirm that a large peak stress in the process zone is attained, which explains why energy amplification by remote plasticity becomes operational and significantly toughens these composites.

## INTRODUCTION

Possibly the most attractive feature of cohesive zone models is their capacity to describe crack growth in elastic-plastic materials with only two parameters, while offering the convenience to separate the contributions to toughness from local fracture energy and from remote plasticity. In a recent paper [1], Brocks pointed out the similarity of cohesive models to Griffith's theory of brittle fracture, and summarized some applications of these models.

The importance of remote plasticity as an amplifier of local cohesive strength was recognized decades ago [2]. Yet, global toughness assessment, such as via the  $J$ -integral, is still dominant, mostly for the experimental convenience of such methods. The shortcomings of these approaches, notably in the presence of extensive plasticity and of substantial crack growth, are nevertheless now apparent [1].

Cohesive modelling faces the challenge of evaluating the local cohesive energy. Basically, two strategies can be defined for its determination: (i) fit of computed load-displacement or  $J$ - $\Delta a$  curves to experimental data, and (ii) computation of the cohesive energy from fracture surfaces, by employing stereophotogrammetric measurements [3].

Typically cohesive zone modelling has been applied to monolithic materials, such as construction steels and aluminium alloys. In this study, we examine bi-phased materials, half-ceramic, half-metal. In a recent paper [4], photoelastic measurements of strain fields ahead of stationary cracks have been presented for such materials. They confirm the presence of extensive plasticity ahead of crack tips. This suggests that an important contribution to toughness comes

from remote plasticity and explains why the toughness of these materials can be quite high, reaching up to  $40 \text{ MPa}\sqrt{\text{m}}$  [5]. Miserez et al. [5] used fractographic analysis in order to evaluate the local fracture energy. The results suggest that the amplification factor is high, on the order of ten. These results are compared in this study with preliminary results from cohesive modelling, conducted by fitting load-displacement curves.

#### EXPERIMENTAL PROCEDURES

The materials are made by gas pressure infiltration of ceramic particle beds. Preforms of angular  $\alpha\text{-Al}_2\text{O}_3$  of  $35 \mu\text{m}$  size (type Alodur™ WSK, Treibacher Schleifmittel, Laufenburg, Germany) or polygonal alumina of  $15 \mu\text{m}$  size (Sumitomo Chemicals Co., Ltd., Tokyo, Japan) are infiltrated with pure (99.99%) aluminium. The resulting metal matrix composites feature a homogeneous microstructure that is free of clusters, voids, veins or other flaws. The volume fraction of reinforcement in the composite is 45% for the angular particles, and 58% for the polygonal particles; such variation in volume fraction is due to the difference of the natural packed density of the two powders.

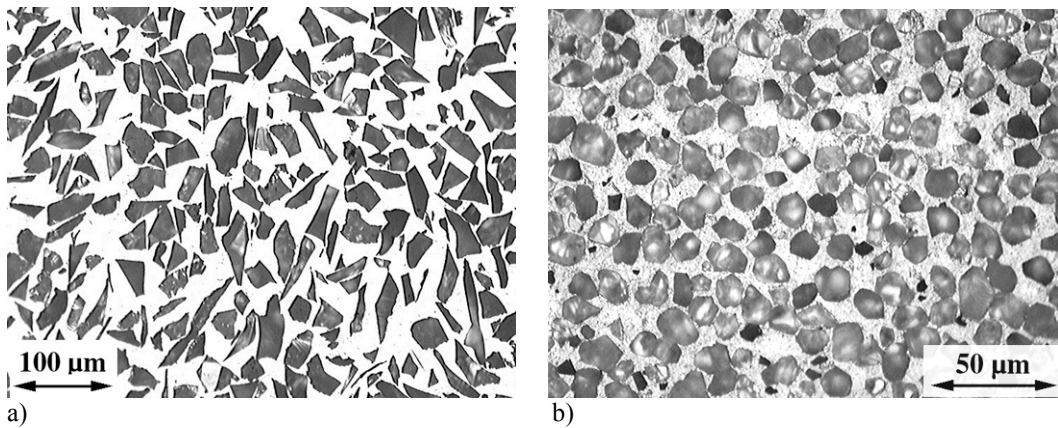


Figure 1: Optical micrographs of the composites. (a)  $35 \mu\text{m}$  angular alumina particles; (b)  $15 \mu\text{m}$  polygonal alumina particles.

Single specimen  $J\text{-}\Delta a$  tests were conducted according to ASTM E-1737. Compact tension (CT) specimens with a width  $W$  of 20 mm were employed. The specimen thickness  $B$  was 13 mm. In order to obtain more homogeneous stress fields in the thickness direction, side-grooves of 20% (i.e. resulting in 10.4 mm specimen net thickness) were machined prior to fatigue pre-cracking. Fatigue pre-cracking was conducted on a 25 kN servohydraulic INSTRON machine. For  $J$ -integral testing, a 100 kN screw-driven Zwick testing frame was employed, at a crosshead velocity of 0.05 mm/min. The stereophotogrammetric measurements were taken on SEM images taken with a Philips XL-30 electron microscope. The three-dimensional reconstruction of fracture surfaces was carried out using the "MEX" software (Alicona Imaging GmbH, Grambach, Austria).

The uniaxial flow behaviour of the composites was studied by tensile testing of flat dogbone specimens. A Zwick 10 kN load frame was employed. Strain rates were varied from nominally  $10^{-8}$  to  $10^{-2} \text{ s}^{-1}$  in order to characterize the strain rate sensitivity of these materials. This has also been examined by San Marchi [6] et al. at higher strain rates.

## MODELLING

Different laws have been proposed in the literature to describe a cohesive zone. Here, we employ Needleman's exponential formulation [7]. To model crack growth in a symmetric CT specimen, only normal loading and separation need to be considered. The cohesive stress reads

$$\sigma_n = \hat{\sigma} \cdot e \cdot z \frac{u_n}{\delta_c} \exp\left(-z \frac{u_n}{\delta_c}\right) \text{ with } e = \exp(1) \text{ and } z = \frac{16 \cdot e}{9} \quad (1)$$

where  $\hat{\sigma}$  denotes the peak normal stress,  $u_n$  the normal separation, and  $\delta_c$  the critical normal separation. The cohesive energy (work of separation per unit area) equals

$$\Gamma = \frac{9}{16} \hat{\sigma} \cdot \delta_c. \quad (2)$$

The cohesive zone model is implemented into the ABAQUS/Standard finite element (FE) code, Version 5.8 (Hibbitt, Karlsson & Sorensen, Inc., Pawtucket, RI, USA) via a user element subroutine. The specimen is modelled in plane strain, using linear elements with "selectively" reduced integration (reduced integration on the volumetric terms). The FE mesh is shown in Fig. 2. The specimen is loaded with a constant displacement rate applied to the triangular elements modelling the pins. A large strain framework is employed for solution. The  $J$ -integral is computed along a line that basically follows the outer contour of the sample (not including the region of the pin hole). The current position of the crack tip is defined as the location of the peak stress.

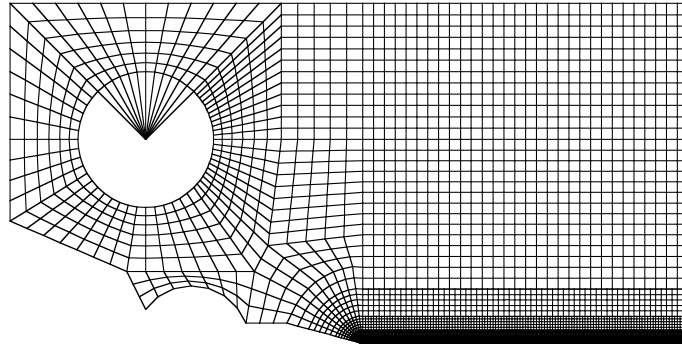


Figure 2: FE mesh of the CT specimen.

The thickness of the plane strain section was chosen to be  $B_e = \sqrt{BB_N}$ , i.e. 11.63 mm. This is a compromise between the equivalent thickness for compliance,  $B_e = B\{1 - (1 - B_N/B)^2\}$ , and the equivalent thickness for the plastic component of the  $J$ -integral,  $B_e = B_N$ . A first loading cycle is carried out until the fatigue pre-cracking load is attained, in order to simulate crack-closure effects resulting from residual stresses.

The surrounding composite material is modelled as homogeneous and isotropic. J2 flow theory is employed. The effective flow curve is described as

$$\sigma = K \cdot \varepsilon_{pl}^n \left(1 + C \cdot \ln \frac{\dot{\varepsilon}_{pl}}{\dot{\varepsilon}_0}\right). \quad (3)$$

The values of the material parameters are summarized in Table 1.

Table 1: Material parameters.

Particle shape and size	$E$ [GPa]	$\nu$	$K$ [MPa]	$n$	$C$	$\dot{\epsilon}_0$ [ $s^{-1}$ ]
angular, 35 $\mu\text{m}$	142	0.3	320	0.21	0.03	$10^{-4}$
polygonal, 15 $\mu\text{m}$	184	0.3	594	0.25	0.03	$10^{-4}$

The inverse problem of fitting the cohesive parameters is solved by an iterative succession of ABAQUS and SiDoLo runs. SiDoLo [8, 9] is a simulation software that compares numerical and experimental results (here load-CMOD curves) evaluates the error functional, and then suggests a new set of parameters till the error reaches a minimum.

## RESULTS

Damage and crack growth in these materials occurs via particle cracking (35  $\mu\text{m}$  angular particles), or matrix voiding (15  $\mu\text{m}$  polygonal particles), each of these followed by tearing of metal ligaments. The polygonal particles, which do not crack, clearly yield a stronger and tougher material. Both materials exhibit stable crack growth. Experimental (not showing the unloading cycles) and computed load vs. CMOD curves are plotted in Fig. 2,  $J$ - $R$  curves in Fig. 3. The fitted parameters of the cohesive law are given in Table. 2. The computations were not run till complete specimen separation, since the cohesive parameters are expected to change for very deep cracks.

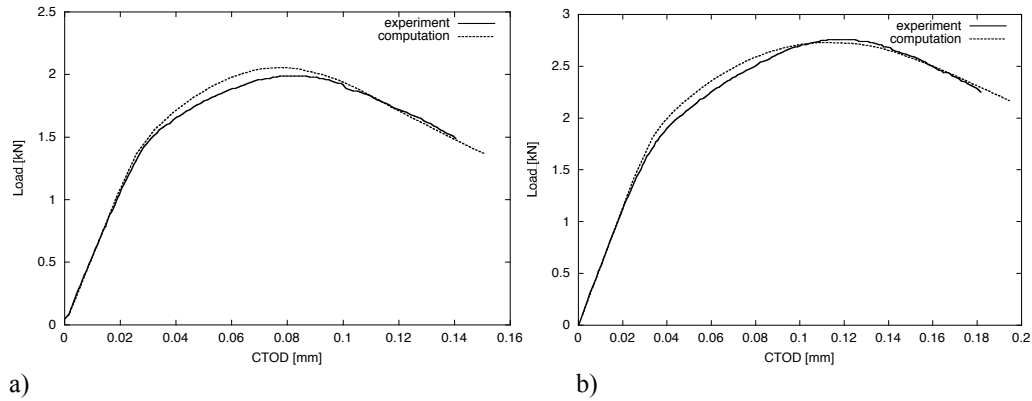


Figure 2: Load vs. crack mouth opening displacement. (a) 35  $\mu\text{m}$  angular reinforcement. (b) 15  $\mu\text{m}$  polygonal reinforcement.

Table 2: Fitted parameters of the cohesive law,  $\hat{\sigma}$  and  $\Gamma$ , local fracture energy values computed from stereophotogrammetric measurements,  $2\gamma_{pz}$ , and experimental  $J$ -values,  $J_{0.2}$  and  $J_{GT}$ .  $J_{GT}$  denotes the value of the  $J$ -integral where a noticeable change of slope occurs [5].

Particle type	$\hat{\sigma}$ [MPa]	$\Gamma$ [N/mm]	$2\gamma_{pz}$ [N/mm]	$J_{0.2}$ [N/mm]	$J_{GT}$ [N/mm]	$J_{GT}/\Gamma$
angular, 35 $\mu\text{m}$	246.7	0.868	0.276	1.9	3.1	3.6
polygon. 15 $\mu\text{m}$	427.6	1.25	0.607	2.8	5.7	4.6

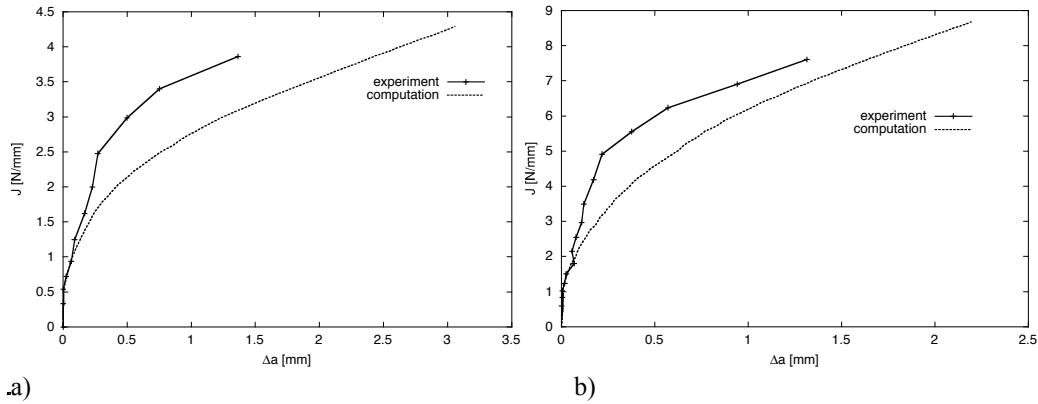


Figure 3:  $J$ - $R$  curves. (a) 35  $\mu\text{m}$  angular reinforcement. (b) 15  $\mu\text{m}$  polygonal reinforcement.

#### DISCUSSION

The preliminary results presented above show both the potential and the weaknesses of the method. Computed  $J$ - $\Delta a$  curves exhibit somewhat stronger crack-advance as compared to experimental curves, notably with the 35  $\mu\text{m}$  angular reinforcement composite. On the other hand, magnitudes and trends are well described. Mainly two reasons can be evoked in order to explain the lack of better agreement: (i) the limited sample dimensions, which do not allow for longer confined crack growth; this would improve the precision in fitting; (ii) the problem of modelling a three-dimensional object in 2-D. The net section thickness in the specimen is 10.4 mm, which is thus the thickness of the crack plane, whereas the nominal specimen section is 13 mm, governing the initial elastic loading part. The compromise chosen for the plane-strain computation can certainly not reflect the true 3-D situation without some error [4]. Another source of uncertainty, though of minor importance, is that the identification of the crack tip with the location of the peak stress is somewhat arbitrary. Finally, although a rate-dependent formulation was chosen for describing the flow stress of the bulk composite material, no rate dependence was assumed for the cohesive law. Unfortunately a rate-dependent cohesive zone requires at least an additional parameter, which reduces the attractiveness of the approach.

On the other hand, our results confirm with sufficient certainty that these half-ceramic metal matrix composites behave essentially like metals, in so far as their fracture toughness is mostly contributed by remote plasticity. As has been pointed out by Tvergaard and Hutchinson [10], such an amplification of toughness is only possible if the peak stress in the process zone equals several times the flow stress. Indeed, our FE results indicate a ratio of  $\hat{\sigma}$  over  $\sigma_{\text{eq}}$  of roughly 4.5, certainly enough for this amplification effect to occur [10]. The values of the local fracture energy computed from stereophotogrammetric measurements are roughly half as large as those fitted for the present cohesive model. Apart from the uncertainty in FE computation, some uncertainty in these experimentally derived values has also to be accounted for: these were derived for uniaxial straining of metal ligaments (resulting from particle cracking and/or matrix voiding), thus neglecting triaxiality (present in the matrix due to plastic constraint by the closely packed ceramic particles) and not incorporating additional dissipation by shear of the soft matrix between hard particles. The "true" amplification factor is probably closer to the values fitted with the cohesive model, i.e. rather five than ten in these materials. This conclusion parallels that of Chen et al. [3]. Finally it is recalled that the local fracture energy can also be identified as the  $J$ -value at crack

initiation, at least in small-scale yielding conditions; however, the steep initial slope of the  $J-\Delta a$  curve and experimental scatter prohibit practical application.

#### CONCLUSIONS

Crack growth was modelled in CT specimens with a cohesive model, whose parameters were fitted from experimental load vs. CMOD records. Computed  $J-\Delta a$  curves exhibit somewhat stronger crack growth as compared to experimental ones. We attribute this offset mainly to the limited sample dimensions, and to the difficulty of representing a 3-D sample with a 2-D plane strain analysis. On the other hand, the agreement is sufficiently good to confirm the metallic character of the examined half-ceramic metal matrix composites, in so far as their toughness is dominated by remote plasticity. The amplification factor in our analysis is about half as large as computed from stereophotogrammetric measurements, but probably more reliable than the latter, which was obtained in a very simplistic analysis. However, both analyses confirm that high peak stresses are necessary and can be obtained in these materials, in order for the energy amplification via remote plasticity to become operational. Ingredients for obtaining tough materials are the absence of processing defects such as voids or veins, the absence of premature interface decohesion and of matrix voiding, and strong reinforcement, all of these features promoting the achievement of higher peak-stresses at the crack tip.

#### REFERENCES

1. Brocks, W., Cohesive strength and separation energy in view of Griffith's concept of fracture, *ESIS Newsletter* 40, 21-30, 2004.
2. Rice, J. R., An examination of the fracture mechanics energy balance from the point of view of continuum mechanics, in *Third Int. Conf. on Fracture*, Sendai, Japan, 309-340, 1965.
3. Chen, R. C., Kolednik, O., Scheider, I., Siegmund, T., Tatschl, A. and Fischer, F. D., On the determination of the cohesive zone parameters for the modeling of micro-ductile crack growth in thick specimens, *Int. J. Fract.* 120, 517-536, 2003.
4. Miserez, A., Rossoll, A. and Mortensen, A., Investigation of crack-tip plasticity in high volume fraction particulate metal matrix composites, *Engng Fract. Mech.* 71, 2385-2406, 2004.
5. Miserez, A., Rossoll, A. and Mortensen, A., Fracture of aluminium reinforced with densely packed ceramic particles: link between the local and the total work of fracture, *Acta Mater.* 52, 1337-1351, 2004.
6. San Marchi, C., Cao, F., Kouzeli, M., and Mortensen, A., Quasistatic and dynamic compression of aluminium-oxide particle reinforced pure aluminium, *Mat. Sci. Engng A* 337, 202-211, 2002.
7. Needleman, A., An analysis of decohesion along an imperfect interface, *Int. J. Fract.* 42, 21-40, 1990.
8. Pilvin, Ph., SiDoLo version 2.4, Notice d'utilisation, Ecole Centrale de Paris, Châtenay-Malabry, France, 1998.
9. Cailletaud, G., Pilvin, Ph., Identification and inverse problems: a modular approach, in MD-43, *Material parameter estimation for modern constitutive equations*, Bertram, L. A., Brown, S. B., and Freed, A. D., eds, ASME, USA, 1993.
10. Tvergaard, V. and Hutchinson, J. W., The relation between crack growth resistance and fracture process parameters in elastic-plastic solids, *J. Mech. Phys. Solids* 40, 1377-1397, 1992.